Express Polymer Letters Vol.16, No.6 (2022) 558–572
https://doi.org/10.3144/expresspolymlett.2022.42

Research article

High-density polyethylene/EPDM rubber blend composites of boron compounds for neutron shielding application

Sajith Thottathil Abdulrahman[1], *Bindu Patanair*[2], *Vineeth Puthuparampil Vasukuttan, Sabu Thomas*[1,7*], *Emmanuel Cadel*[2], *Fabien Cuvilly*[2], *Allisson Saiter-Fourcin*[2], *Zakiah Ahmad*[3], *Maciej Jaroszewski*[4], *Michal Strankowski*[5], *David Laroze*[6]

[1]School of Energy Materials, International and Inter University Centre for Nanoscience and Nanotechnology, School of Chemical Sciences, Mahatma Gandhi University, Priyadarsini Hill (PO), 686 560 Kottayam, Kerala, India
[2]Normandie Univ, UNIROUEN, INSA Rouen, CNRS, GPM, 76000 Rouen, France
[3]Faculty of Civil Engineering, Universiti Teknologi Mara, 40450 Selangor, Malaysia
[4]Faculty of Electrical Engineering, Wroclaw University of Science and Technology, Wybrzeze Wyspianskiego 27, 50-370 Wroclaw, Poland
[5]Gdańsk University of Technology, Chemical Faculty, Polymer Technology Department, room 210a, ul. G. Narutowicza 11/12,80-233 Gdańsk, Poland
[6]Instituto de Alta Investigación, Universidad de Tarapacá, Calle Antofagasta 1520, Casilla 7D, Arica, Chile
[7]Department of Chemical Sciences, University of Johannesburg, P.O. Box 17011, Doornfontein, 2028, Johannesburg, South Africa

Received 14 September 2021; accepted in revised form 1 February 2022

Abstract. Novel materials with neutron shielding property were fabricated by incorporating boron compounds into high-density polyethylene (HDPE)/Ethylene propylene diene monomer rubber (EPDM) blends. A detailed investigation on the morphological, thermal, mechanical, and neutron attenuation properties of suitable proportion of HDPE/EPDM blend with boric acid (BA), boron carbide (BC), and nano boron carbide (NBC) were performed. Morphology of the 20 wt% of EPDM shows better distribution in HDPE matrix. BA filler is localised in the HDPE phase, while NBC shows uniform distribution in HDPE/EPDM blend compared to its micro counterpart. There is a reduction in the tensile strength and modulus with the incorporation of EPDM in HDPE, whereas the ductility of HDPE is enhanced. A significant increase in the tensile toughness of the HDPE/EPDM blend with lower tensile strength and modulus is observed for BA, and BC filled composites. Moreover, HDPE/EPDM composites with NBC show only a marginal increase in the tensile toughness, tensile strength, and modulus. Comparison of the Young's modulus of the HDPE/EPDM blends with theoretical models indicates trends similar to the Coran model. The BA and BC filled composites follow the lower bound series model, whereas NBC composites show behaviour similar to the Halpin Tsai model. Total thermal neutron macroscopic cross-section (0.025 MeV energy neutrons) of 10 cm^{-1} and mean free path of 0.1 cm was obtained for 20 wt% NBC HDPE/EPDM composites.

Keywords: *thermal properties, borated polymers, thermoplastic elastomers, neutron shielding, mechanical properties*

1. Introduction

Nuclear radiations are unavoidable in nuclear reactors, medical field, and aerospace industries, whereas unwanted radiation is harmful to human beings, living organisms as well as the environment [1, 2]. To ensure the safety of workers and the general public, all nuclear-related activities should be applied with the radiation safety principle called 'ALARA' or 'As Low As Reasonably Achievable' [3–5]. In this regard, the demand for a reliable neutron radiation

*Corresponding author, e-mail: sabuthomas@mgu.ac.in

shielding material has been developed during the last decade.

Materials that are rich in hydrogen are good in decelerating the fast neutrons and further can be absorbed with elements whose thermal neutron absorption is high such as boron, lithium, rare earth metals, *etc*. [6, 7]. High-density polyethylene (HDPE) based multifunctional composites were widely used for neutron shielding due to their high hydrogen content [7]. Boron compounds are good in abundance, cost-effective, and have high absorption cross-sections [8]. Boron compounds are usually incorporated into the HDPE to enhance the neutron absorption property of the material. The distribution of boron compounds and their interaction with the HDPE matrix are the major factors influencing the neutron shielding properties. Boric acid (BA) is commonly used as a cheap neutron-absorbing filler with a layered structure. Boron carbide (BC) is a hard boron compound with a rhombohedral structure with boron atoms at the corners. Both BA and BC fillers are abundant and cost-effective when compared with boron nitride (BN).

The influence of the boron compound particle size in its distribution is another factor that improves the neutron shielding properties. Kim and coworkers [9, 10] investigated the effect of nano-sized Boron Carbide (NBC) on the properties of the HDPE composites. The macroscopic cross-section of HDPE/BC composites was higher for the NBC when compared with the micro counterparts. The size reduction of BC to nanosize by ball milling process helps in the uniform distribution of fillers in the HDPE matrix. This, in turn, enhanced the mechanical and neutron shielding characteristics of NBC/HDPE composites. Boron-doped MWCNT/HDPE nanocomposites show a macroscopic cross-section of 106 m^{-1} with high tensile characteristics [11]. HDPE/BN composites were analyzed for spacecraft radiation shielding [12]. The surface modification of the BN improved the adhesion with matrix and increased the mechanical properties, thereby achieving radiation shielding efficiency similar to that of aluminum. In another report, better distribution for silane-modified BN/ HDPE composites with an increase of 23% more than unmodified composites was observed [13]. These studies show the influence of filler size, its distribution, and filler-matrix interaction on the neutron attenuation property of the materials. Nevertheless, low toughness, heat resistance, and flammability are the drawbacks of HDPE; those are significant in terms of material application [14].

Researchers have shown great interest in thermoplastic elastomer-based neutron shielding materials because of their tailorable nature. Thermoplastic elastomeric materials based on blends of HDPE and ethylene propylene diene monomer rubber (EPDM) combine the technical advantages in the processing of thermoplastics with the excellent physical properties of elastomers, thus, gaining significant importance in a wide range of applications. EPDM-based composites were extensively studied because of their neutron and gamma radiation shielding properties [15, 16]. The blends of EPDM/LDPE (50/50) with 47 and 57% BC displayed a macroscopic cross-section of 0.215 cm^{-1} for slow neutrons and temperature independent enhancement in thermal and electrical properties with BC filler addition [17]. The NR/HDPE/liquid natural rubber with varying BC fillers indicated the importance of filler concentration role in improving neutron absorption and mechanical properties [18]. Thermoplastic natural rubber (TPNR) with varying BC composites showed an increase in macroscopic cross-section from 3.34 up to 14.8 cm^{-1} with BC loading [19]. However, despite these few reports, no systematic studies were conducted to find the influence of boron compounds in thermoplastic elastomers such as HDPE/EPDM composites.

In this context, our aim was to develop HDPE/EPDM composites with varying boric acid and boron carbide. The morphological and mechanical properties of HDPE/EPDM composites were analyzed, and the mechanical properties were compared with theoretical models. The influence of fillers on the neutron shielding characteristics were also studied.

2. Materials and methods

2.1. Materials

High-density polyethylene (HDPE) of HD50MA180 was purchased from Reliance Polymers, India, Ethylene-propylene diene monomer rubber (EPDM) of Keltan® 9565Q procured from LANXESS Elastomers (ethylene content 62 wt%), Trimethyl quinone of industrial-grade from Sameera chemicals, India. The neutron-absorbing fillers viz. boric acid 99.50% purity was purchased from Nice Chemicals, India; BC of 98% purity and particle size <10 μm was purchased from Sigma Aldrich and NBC of <500 nm size was from GetNanoMaterials, France.

2.2. Preparation

Initially the EPDM concentration is varied for 0 up to 40, and corresponding samples were termed as EP 0, EP 10, EP 20, EP 30, and EP 40 according to the EPDM [wt%]. Furthermore, to understand the influence of neutron absorbers, boric acid, BC, and NBC were varied in the EP 20 (HDPE/EPDM (80/20)) sample. The boric acid filled composites were termed as BA 0, BA 5, BA 10, and BA 15, corresponding to boric acid [wt%] varies from 0 up to 15. Similarly, BC and NBC were termed as BC 10, BC 20, BC 30, NBC 5, NBC 10, and NBC 20 for their corresponding [wt%]. HDPE/EPDM with varying neutron absorbers was prepared by using a Brabender internal melt mixer at 150 °C for 10 min with a rotor speed of 60 rpm. The mixing sequence involved first introducing HDPE into the mixer and after melting HDPE (3 min), the EPDM rubber was added for (2 min) followed by the addition of antioxidant TQ (1 min). The mixing was continued for 4 min, and the final material was compounded in a compression molding machine at 170 °C for 5 min.

2.3. Characterization techniques

Morphological analysis was carried out using a Scanning Electron Microscope (JEOl-JSM 7900F). The cryofracture surfaces of the samples were coated with carbon using Cressington 108 Carbon/A carbon coater instrument and observed under SEM to know the dispersion and distribution of EPDM and fillers in HDPE.

Dumbbell-shaped samples were cut from the molded sheets, and the samples were subjected to tensile testing at a crosshead speed of 50 mm/min using a H25K type universal testing machine (Tinius Olsen, UK). The characteristics like tensile strength [MPa], elongation at break [%], Young's modulus [MPa] were found according to ASTM D-638.

In order to study the thermal stability of the different samples, thermogravimetric analyses (TGA) were carried out using a TGA 209 Netzsch instrument. The analyses were performed under nitrogen (25 ml/min) in the 25–800 °C range, at 10 °C/min scanning rate, on 5–10 mg samples. From the analysis of the thermograms, the onset degradation temperature (T_{onset}), which is the temperature corresponding to approximately 3 up to 8 % mass loss, and the final residue at 800 °C were determined.

In order to study the microstructure by evidencing the ability to crystallize under cooling and by calculating the crystallinity degree, classical Differential Scanning Calorimetry (DSC) experiments were conducted on a thermal analysis instrument heat flow calorimeter (DSC Q100 TA Instrument®), coupled with a Refrigerated Cooling System (RCS). The experiments were conducted under an inert nitrogen atmosphere with a flow of 50 ml/min. The apparatus was calibrated for heat flow, temperature, and baseline using standard Tzero technology. For temperature calibration, a standard Indium (T_m = 156.60 °C and ΔH_m = 28.38 J/g) sample was used. The DSC analyses of all the samples were carried out from –90 up to 250 °C at a heating rate of 10 °C/min. Just before the cooling ramp, an isotherm at 250 °C for 5 min was performed for all the samples in order to erase the thermal history. The cooling rate was chosen equal to the heating one. The 1st heating of all the samples was discarded; data related to cooling and second heating are considered in this work.

3. Result and discussion

3.1. Morphology analysis

Scanning electron microscopy images of the EPDM/HDPE blends with different EPDM addition are represented in Figure 1.

From the literature reports, it was understood that EPDM appears as a dispersed phase and HDPE as a matrix phase at lower EPDM concentrations [20]. It is observed that the surface of HDPE was very smooth due to its crystalline nature. Upon incorporation of EPDM, the surface appears irregular, and the EPDM appears as spherical shapes with nonuniform boundaries in Figure 1b. In Figure 1c the EPDM is clearly visible as dark phases, which were distributed in the HDPE matrix. A similar distribution of EPDM in the HDPE matrix was also noticed from the AFM topographies of EPDM/HDPE blends by Stelescu *et al*. [21].

The addition of boric acid to the best concentration EP 20 appears as white spots in the SEM images (see Figure 2). With 5 wt% of BA addition, the particles are uniformly dispersed and distributed over the blend, but with 15 wt% of BA, slight agglomeration of BA particles can be seen in the blended composite. Moreover, the droplets of EPDM are clearly visible with BA fillers surrounding it, which shows the fillers are localized only in the HDPE phase, as seen in Figure 2c. Figure 2d shows surface images of 10 wt% and Figure 2e show 20 wt% BC filler loaded

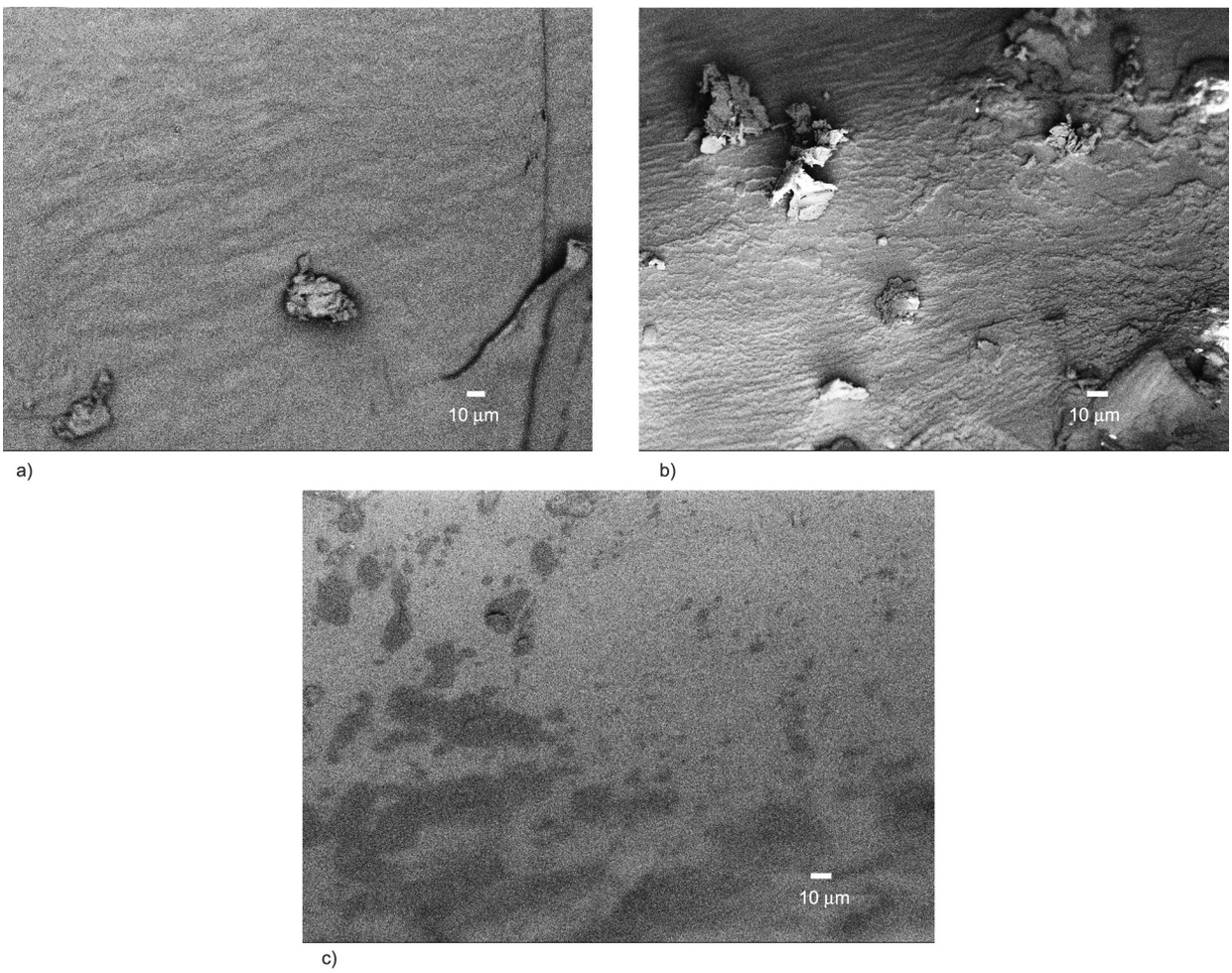

Figure 1. Cryo-fractured surface images of the HDPE/EPDM blends with varying EPDM content (a) EP 0, (b) EP 20, (c) EP 40.

in the blends. Irregular morphology with non-uniform distribution of BC fillers in the HDPE/EPDM blends with larger particle size is evidenced from the images. BC fillers appear as triangular shapes because of their rhombohedral structure. The surface images of the NBC-filled composites are shown in Figure 2f. Unlike BC filled composites, nanocomposite surfaces are smooth and show uniform distribution. Reduction in wrinkles is noticed in the morphology of 10 wt% NBC composites Figure 2g shows the enhanced compatibility of NBC with the blend. In the meantime, particle size increases in the case of 20 wt% NBC filler loaded composites (Figure 2g). This can be due to the aggregation of NBC in the polymer matrix, which occurred during mixing. Also, nano BC of diameter less than 0.5 µm are visible.

3.2. Thermal analyses

Results concerning the TGA analyses are presented in Figure 3. Figure 3a shows the evolution of the % weight as a function of temperature for the different systems.

All the nanocomposites exhibit a clear one-step weight loss process except BA 5 and BA 15; these two samples follow a two-step weight loss process and exhibit a small weight loss at 150 °C (2%), maybe due to the presence of moisture in it [22]. In all the cases, major weight loss occurs around the temperature range 400–515 °C. After 515 °C, there is no weight loss, and all the thermograms remain at a plateau. The temperature corresponding to the onset of degradation T_{onset} and maximum degradation T_{max} are presented in Table 1 EP 0 exhibits the onset of degradation at 415 °C, maximum weight loss at 483 °C, and after 515 °C there is no degradation. This behavior is in good agreement with a previous report [23]. This single-stage degradation at 515 °C can be attributed to the decomposition of –C–C– backbone of polyethylene chain [23].

Figure 3b shows the derivative curves of samples containing BA, which helps to understand the two-step

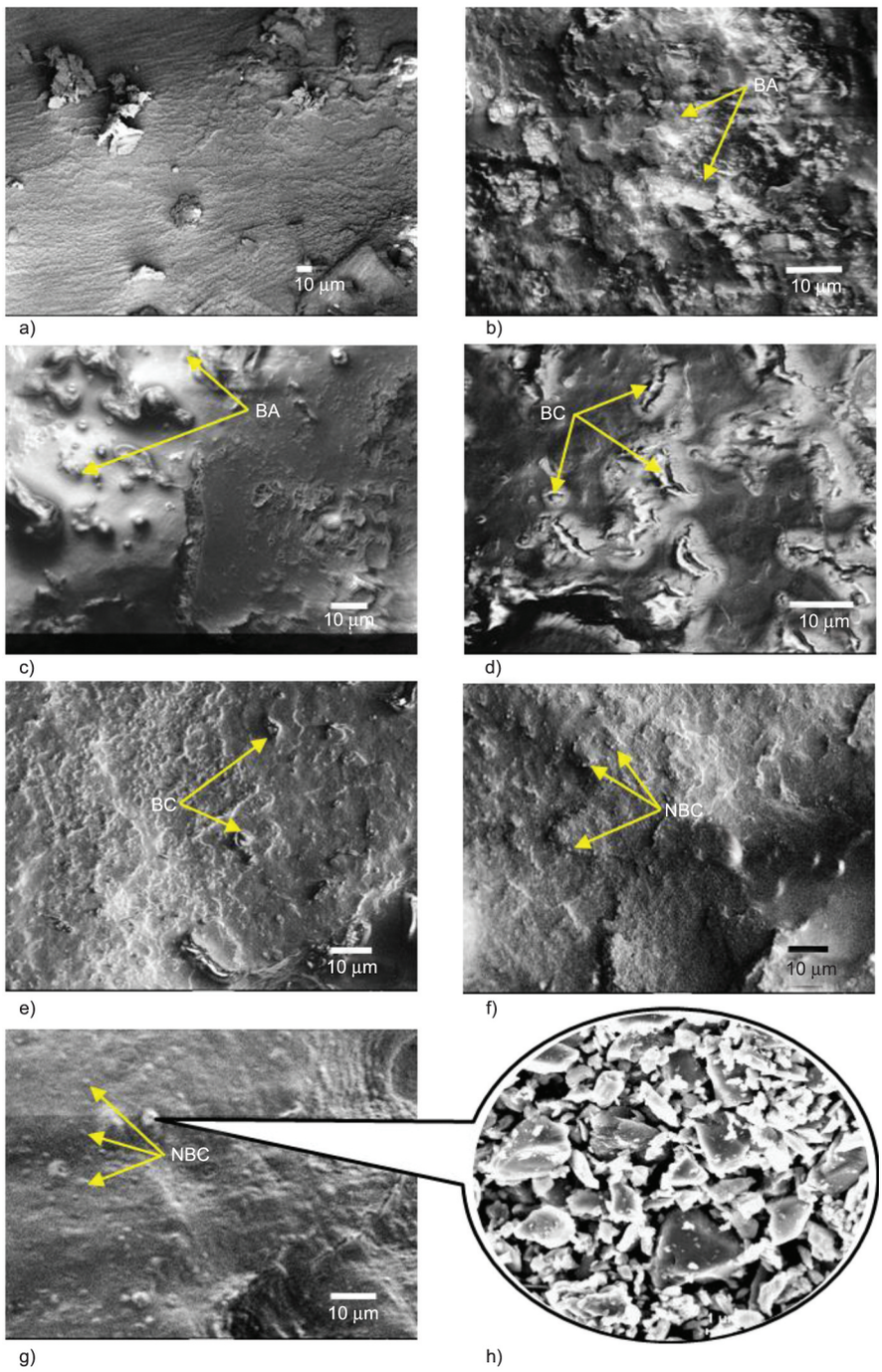

Figure 2. Cryo-fractured surface images of the HDPE/EPDM composites with varying BA, BC, and NBC content (a) EP 20, (b) BA 5, (c) BA 15, (d) BC 10, (e) BC 20, (f) NBC 10 and (g) NBC 20, (h) NBC particles alone.

weight loss process as well as to determine the temperature at which the degradation velocity is maximum (T_{max}).

From Table 1, it can be concluded that the thermal stability of the HDPE is influenced by the presence of the fillers and not by EPDM. Furthermore, the % residues at 650 °C correspond to the amount of fillers. TGA analysis is an interesting technique to check the filler content in composite materials.

Before studying the mechanical properties, it is important to check the influence of the fillers and EPDM on the HDPE ability to crystallize. DSC analyses have been performed to study the crystallization process. Figure 4 presents the calorimetric signatures of each sample during the heating (Figure 4a) and the cooling (Figure 4b) ramps. All the quantities extracted from DSC experiments (*i.e.* the melting temperature taken at the peak maximum T_{mmax}, the crystallization

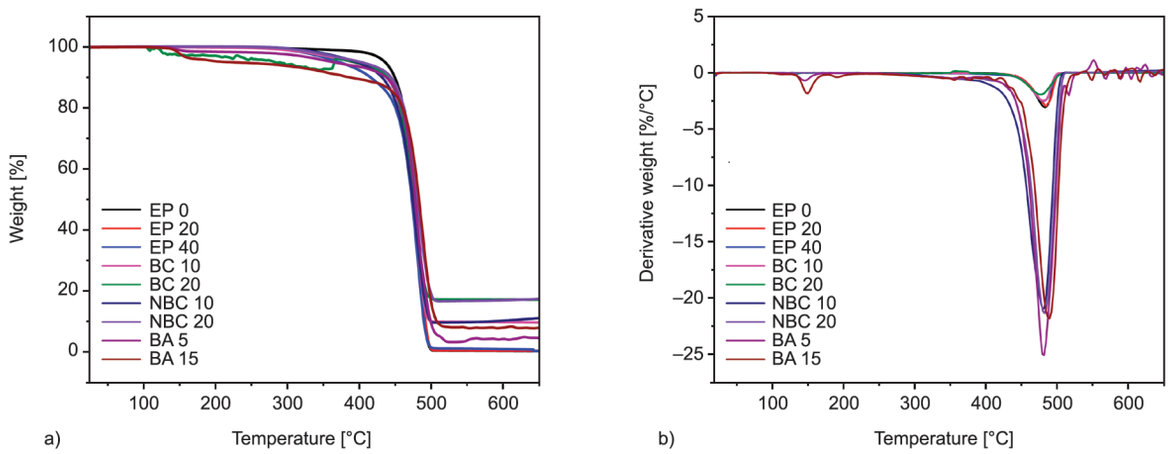

Figure 3. Thermogravimetric analyses under Nitrogen: (a) weight percent and (b) derivative of weight percent as a function of the temperature.

temperature taken at the peak maximum T_{cmax}, the melting and crystallization enthalpies respectively noted ΔH_m and ΔH_c, and the crystallinity degree X_c) are given in Table 2.

Table 1. Thermogravimetric analyses under Nitrogen: Temperature of degradation taken at the onset T_{onset}, residue in percentage at 650 °C, and temperature of degradation taken at the maximum of the peak on derivative curves T_{max}. The precision of the temperature measurements is 1 °C.

Samples	T_{onset} [°C]	Residue at 650 °C [%]	T_{max} [°C]
EP 0	415	0	483
EP 20	408	0	483
EP 40	400	0	483
BC 10	411	10	480
BC 20	410	18	479
NBC 10	408	10	480
NBC 20	415	18	480
BA 5	410	5	480
BA 15	410	9	483

Pure HDPE (*i.e.*, EP 0 sample) exhibits melting and crystallization peaks at 128 and 107 °C, respectively,

Table 2. DSC Parameters of HDPE/EPDM blends and its composites. T_{mmax}: melting temperature taken at the peak maximum, T_{cmax}: crystallization temperature taken at the peak maximum, ΔH_m and ΔH_c: the melting and crystallization enthalpies respectively and calculated by normalizing the areas under the peaks to the HDPE mass, X_c: crystallinity degree calculated from $X_c = \Delta H_m/\Delta H_{m0}$ with $\Delta H_{m0} = 296$ J/g [24]. The precision of the X_c values is 5 %.

Samples	T_{mmax} [°C]	T_{cmax} [°C]	ΔH_m [J/g]	ΔH_c [J/g]	X_c [%]
EP 0	128.3	107.6	180	178	61±5
EP 20	127.1	103.2	175	165	59±5
EP 40	125.8	104.4	180	162	61±5
BC 10	126.8	106.4	157	150	53±5
BC 20	127.4	105.8	150	141	51±5
NBC 10	126.9	108.4	161	156	54±5
NBC 20	127.5	104.0	149	144	50±5
BA 5	127.0	109.4	162	157	55±5
BA 15	126.8	109.7	157	152	53±5

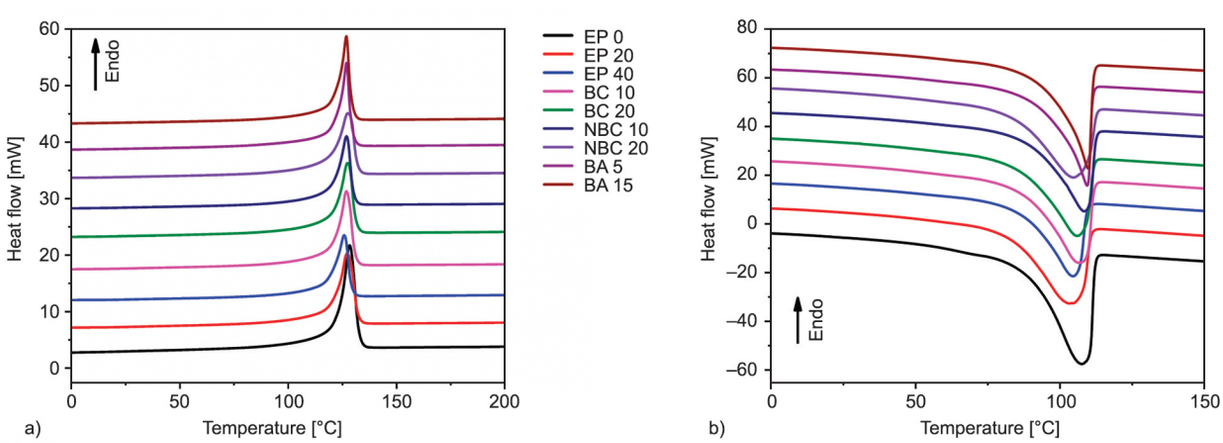

Figure 4. DSC analyses: evolution of heat flow as a function of temperature for (a) 2nd heating and (b) cooling.

with a crystallinity degree of 60%. All these values are consistent with those of the literature for this well-known polymer [24]. The addition of EPDM (*i.e.*, EP 20 and EP 40 samples) has no clear influence on the crystallization and the melting behaviours of HDPE. This is due to the incompatibility between HDPE and EPDM [24]. The comparison between the EP 20 blend sample and its composites gives evidence that there is no noticeable influence on the ability to crystallize and on the degree of crystallinity due to the presence of fillers, whatever be the nature and the content of these fillers.

To conclude about DSC analyses, there are no significant changes evidenced in terms of the degree of crystallinity between the different samples. Thus, if changes will be evidenced in terms of mechanical properties, they will not be due to the crystalline phase but due to the nature and/or to the amount of the fillers.

3.3. Mechanical properties

The tensile plots of the blends are shown in Figure 5, and the corresponding parameters are tabulated in Table 3. The tensile strength, yield stress, and Young's modulus show a remarkable decrease for the binary blends (EP 10, EP 20, EP 30, and EP 40) compared to neat HDPE due to the increase in soft rubbery phase in the matrix [20, 21]. A noticeable increase in the elongation at break occurred at 20 wt% EPDM addition with reduced tensile strength and modulus.

Table 3. Tensile properties of the HDPE/EPDM blends and composites with varying EPDM, BA, BC and NBC concentrations.

Sample code	Young's modulus [MPa]	Tensile strength [MPa]	Elongation at break [%]	Toughness [kJ/m^3]
EP 0	275.8±32	20.6±0.15	10.5±0.5	165.5±22
EP 10	215.8±8	14.1±0.1	10.6±0.1	135.9±13
EP 20	201.1±6	10.9±0.55	24.9±0.45	262.1±9
EP 30	91.9±4	7.4±0.43	34.6±1.2	249.4±11
EP 40	72.8±9	5.4±0.21	44.3±3.6	247.7±15
BA 5	263.3±28	12.3±0.46	12.4±2.8	166.1±13
BA 10	284.0±11	11.0±0.58	13.2±3.4	174.3±16
BA 15	285.5±2	8.7±0.15	5.7±0.33	47.8±4
BC 5	296.2±1	11.7±0.2	10.1±1.6	126.6±3
BC 10	236.3±9	11.4±0.17	14.7±0.9	85.3±7
BC 20	267.8±23	11.2±0.13	10.9±3.4	108.8±10
NBC 5	279.7±31	12.1±0.11	22.6±1.4	255.5±11
NBC 10	282.3±20	11.7±0.17	21.1±3.2	259.4±8
NBC 20	291.3±14	12.2±0.15	18.6±4.2	228.8±12

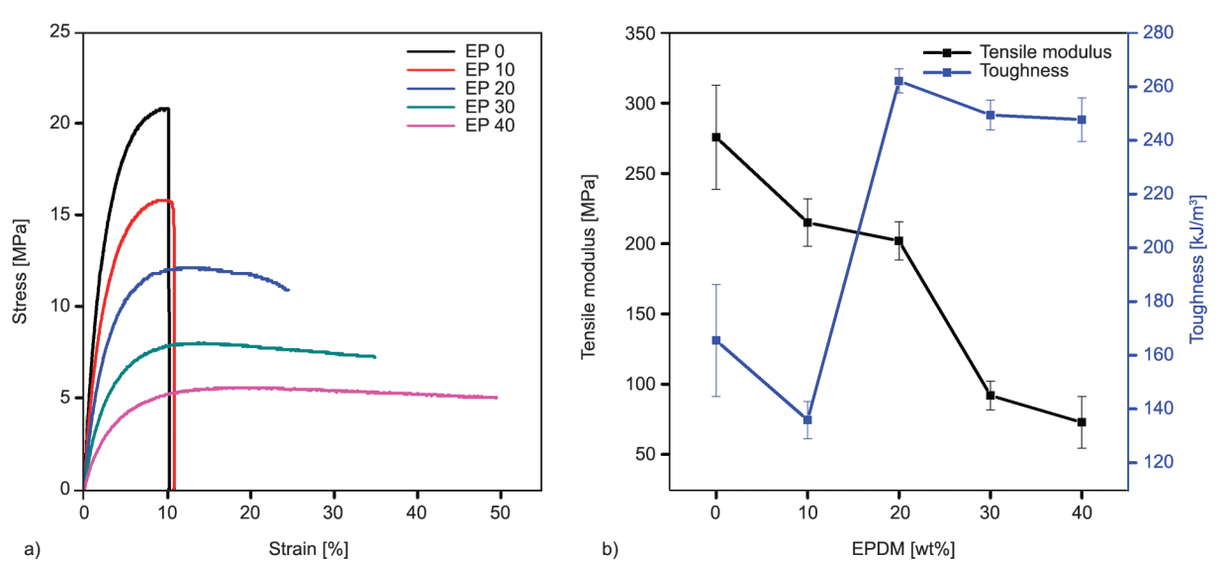

Figure 5. a) Stress-strain curves and b) tensile modulus and toughness of HDPE/EPDM blends with varying EPDM content.

The increase in EPDM [wt%] facilitates the tensile ductility of the material, and that causes the enhancement in the elongation at break [%] [25].

The area under the stress-strain curve represents the tensile toughness (total strain energy/unit volume) [26] of the composite, which increases with EPDM content and that resembles the increase in the toughness of the blends. Weak interfacial interaction at 10 wt% EPDM concentration causes reduced toughness due to the localized and non-uniform distribution of dispersed EPDM phase [24]. The toughness of the 20 wt% EPDM incorporated blend is improved by 58% compared to neat HDPE, and further loading leads to a marginal decrease. The suitable particle size of the elastomer and good interfacial interaction are the major factors affecting the toughness of the material [27].

The blend composition with 20 wt% EPDM content shows a tensile strength of 12 MPa, the toughness of 262 kJ/m^3, and an elongation of 25%, has been selected for further addition of neutron-absorbing fillers BA, BC, and NBC. The stress-strain plots of the BA-filled composites are represented in Figure 6, and the parameters extracted from these investigations are given in Table 3.

The introduction of 5 wt% boric acid in HDPE/EPDM blend enhances the tensile strength and modulus by 7.4 and 15 %, respectively, as represented in Figure 6. Up to 10 wt% of BA addition in the blends, the tensile strength and modulus are higher than blends without boric acid. The increase in the tensile strength and Young's modulus can be due to the layered structure and crystalline nature of boric acid [22]. Similar observations were also noticed for layered fillers such as clay, layered hydroxides, and graphene plates in the thermoplastic elastomers, in which the tensile properties improved at lower concentrations of fillers [28–30]. The decrease in the tensile strength and modulus beyond the 10 wt% addition of boric acid fillers may be caused by the agglomeration as observed from the SEM images. The elongation at break [%] and the tensile toughness show significant reduction at 15 wt. % BA loading, which suggests weak interfacial interaction among the HDPE/EPDM/ boric acid ternary systems. The BA aggregation at the HDPE/EPDM interface can act as stress concentration sites which causes early failure to applied tensile load [31].

The stress-strain plots of the hardest and rhombohedral structured BC filled HDPE/EPDM composites are shown in Figure 7. It is found that the tensile strength and modulus of the HDPE/EPDM composites marginally increased with the incorporation of BC. The BC filler increases the stiffness of the composite due to its hardness and reinforcing nature [32]. On the other hand, a substantial reduction in the elongation at break [%] is observed with BC loading. Unlike rigid fillers, carbon black, and SiO_2 in the HDPE-based matrix, the sharp edges of the BC cause filler-matrix debonding with the applied tensile force [33, 34]. The toughness of the composites declines by 26% for the 20 wt% BC containing composites, that may have occurred due to the poor stress transfer to the external load.

The incorporation of nano NBC enhances the tensile characteristics expressively, as illustrated in Figure 8.

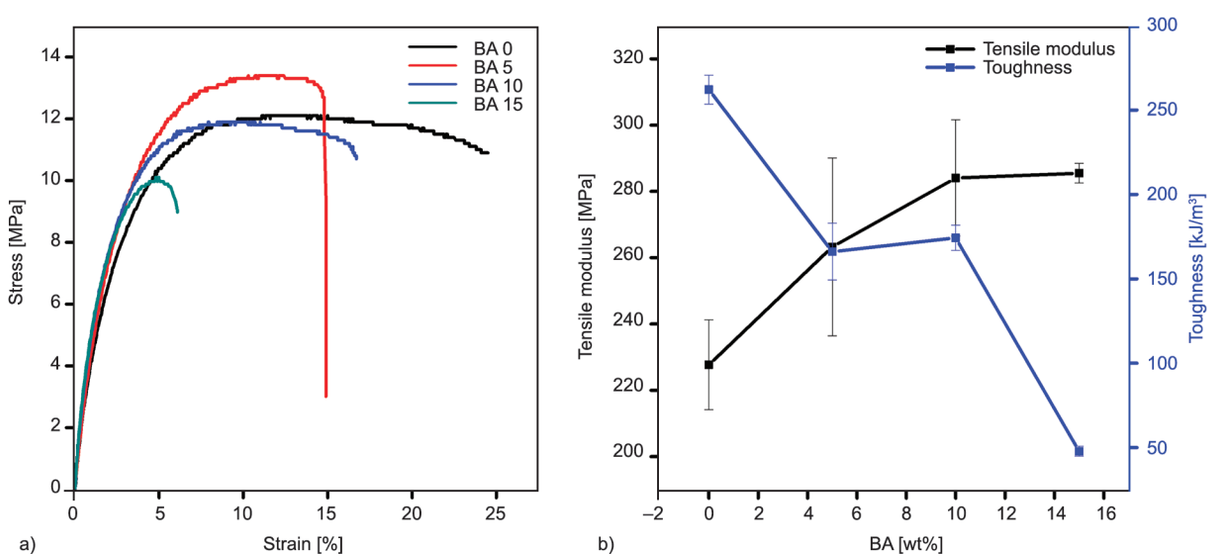

Figure 6. a) Stress-strain curves and b) tensile modulus and toughness of HDPE/EPDM/boric acid with varying boric acid content.

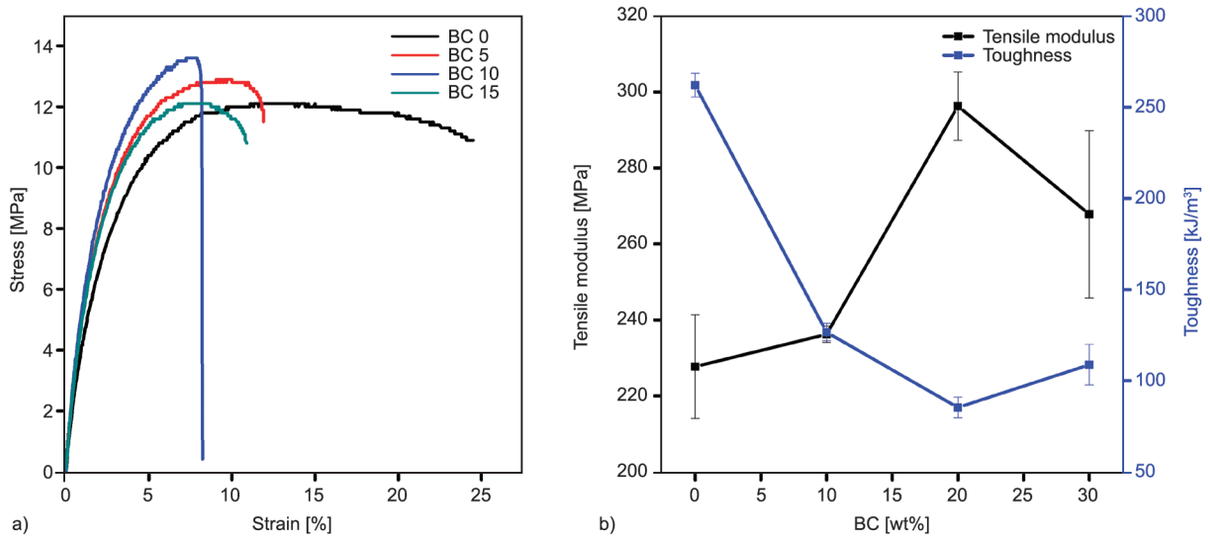

Figure 7. a) Stress-strain curves and b) tensile modulus and toughness of HDPE/EPDM/BC with varying BC content.

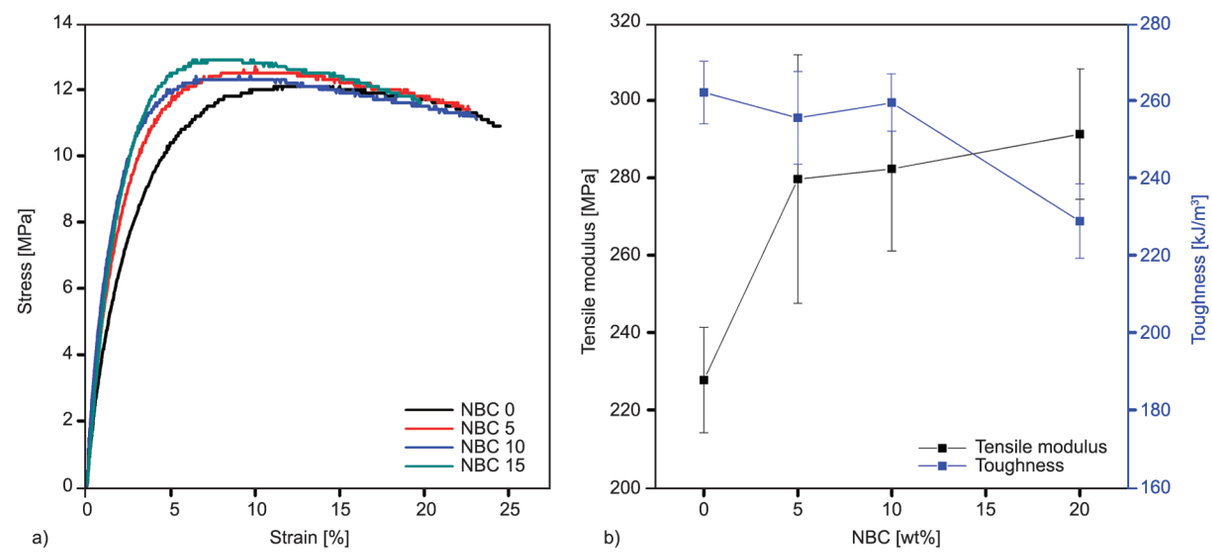

Figure 8. a) Stress-strain curves and b) tensile modulus and toughness of HDPE/EPDM/NBC with varying NBC content.

The enhanced surface area and uniform distribution achieved because of the nanosize of the BC is the reason for the improved properties [10]. The tensile strength and modulus of the composites show significant improvement with the wt% of NBC. The addition of 20 wt% NBC increases the tensile strength and modulus by 6.5 and 28%, respectively. The increment in the modulus [%] with NBC is lower compared to the studies of Harrison *et al*. [33] and Kim *et al*. [10], which indicates the uniform distribution of NBC in both phases of HDPE and EPDM. Unlike BC-filled composites, an only marginal decrease in elongation at break is observed that shows the better compatibility between the NBC and HDPE/EPDM blends. This indicates the large surface area and reduced size of the NBC particles and better compatibility in the HDPE/EPDM blend system. Also, the toughness of the blends indicates only marginal reduction with NBC addition. The morphological changes occurring in the EP 20, BC 10, and NBC 10 filled HDPE/EPDM composites, to the applied tensile forces, were represented schematically in the Figure 9.

3.4. Theoretical models

The Young's modulus of the composites can be predicted by several models such as Parallel, Series, Coran, and Halpin Tsai models [35, 36]. These models are based on the dependence of the composition and morphology in the composites. The simplest models are parallel (Equation (1)) and series (Equation (2)) models that represent the upper and lower bounds of Young's modulus. The strain is assumed to be constant in the parallel model, while stress is

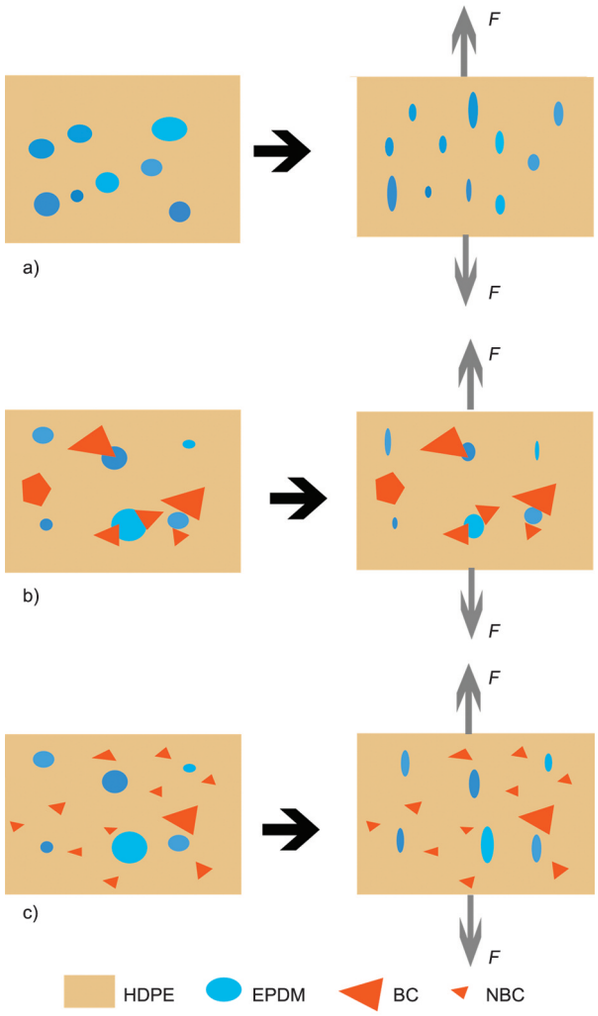

Figure 9. Schematic representation of the morphological changes occurring to the applied tensile forces of a) EP 20, b) BC 10 and c) NBC 10 composites.

assumed as uniformly distributed in the series model. The shape and size of the dispersed phase and the interfacial interactions are not considered in these models:

$$E_c = E_1\Phi_1 + E_2\Phi_2 \tag{1}$$

$$\frac{1}{E_c} = \frac{\Phi_1}{E_1} + \frac{\Phi_2}{E_2} \tag{2}$$

where E_c is property of the composite in which E_1 and E_2 are Young's modulus, and Φ_1 and Φ_2 are the volume fractions of the components, respectively.

Coran suggests that the variation of Young's modulus with incompatible fillers will be in-between the parallel [E_p] and series [E_s] models (Equation (3) and (4)):

$$E_c = f\left(E_p - E_s\right) \tag{3}$$

$$f = \Phi_h^n\left(n\Phi_s + 1\right) \tag{4}$$

where f is a factor that varies between 0 to 1 and Φ_h and Φ_s are volume fractions of hard and soft phases, respectively.

Moreover, the Halpin Tsai equation is widely used to study the effect of filler reinforcement with continuous and discontinuous phases in the composites that are oriented in the loading direction. According to Halpin Tsai, the tensile properties of the reinforced composites are shown in the Equation (5):

$$E = E_m\frac{1 + \xi\eta\Phi}{1 - \eta\Phi} \tag{5}$$

where the shape parameter (ξ) of the filler is accounted for, and η is given by Equation (6) in which Young's modulus of the filler is represented as E_f:

$$\eta = \frac{\frac{E_f}{E_m} - 1}{\frac{E_f}{E_m} + \xi} \tag{6}$$

If the filler orientation is perfect, the shape factor $\xi = 2$ (width/thickness), of the filler. Since E_f is much higher than E_m, its value is nearly equal to 1.

The experimental Young's modulus of the blends and composites as a function of volume fractions of fillers were compared with the above models and represented in Figure 10.

The experimental Young's modulus of EPDM volume fractions in EPDM/HDPE blends (Figure 10a) was identical to the Coran model except at 0.2 volume fraction. One can notice at 0.2 volume fraction, Young's modulus shows behavior similar to the upper bound parallel model in which strain in HDPE and EPDM phases is considered as constant [37]. This indicates the better distribution of EPDM rubber in the HDPE matrix at 0.2 volume fraction (20 wt%) of EPDM loading.

The incorporation of BA and BC volume fractions in the EPDM/HDPE composites shows the trends similar to lower bound series models Figures 10b and 10c. The incompatibility among the ternary blend system of HDPE, EPDM, and BA or BC, may result in the distribution of EPDM and BA or BC in such a way that applied tensile stress is constant. Whereas the NBC-filled composites resemble a trend similar to Halpin Tsai behavior, as shown in Figure 10d. The influence of the shape parameters of the fillers plays a major role in the Halpin Tsai model, which suggests

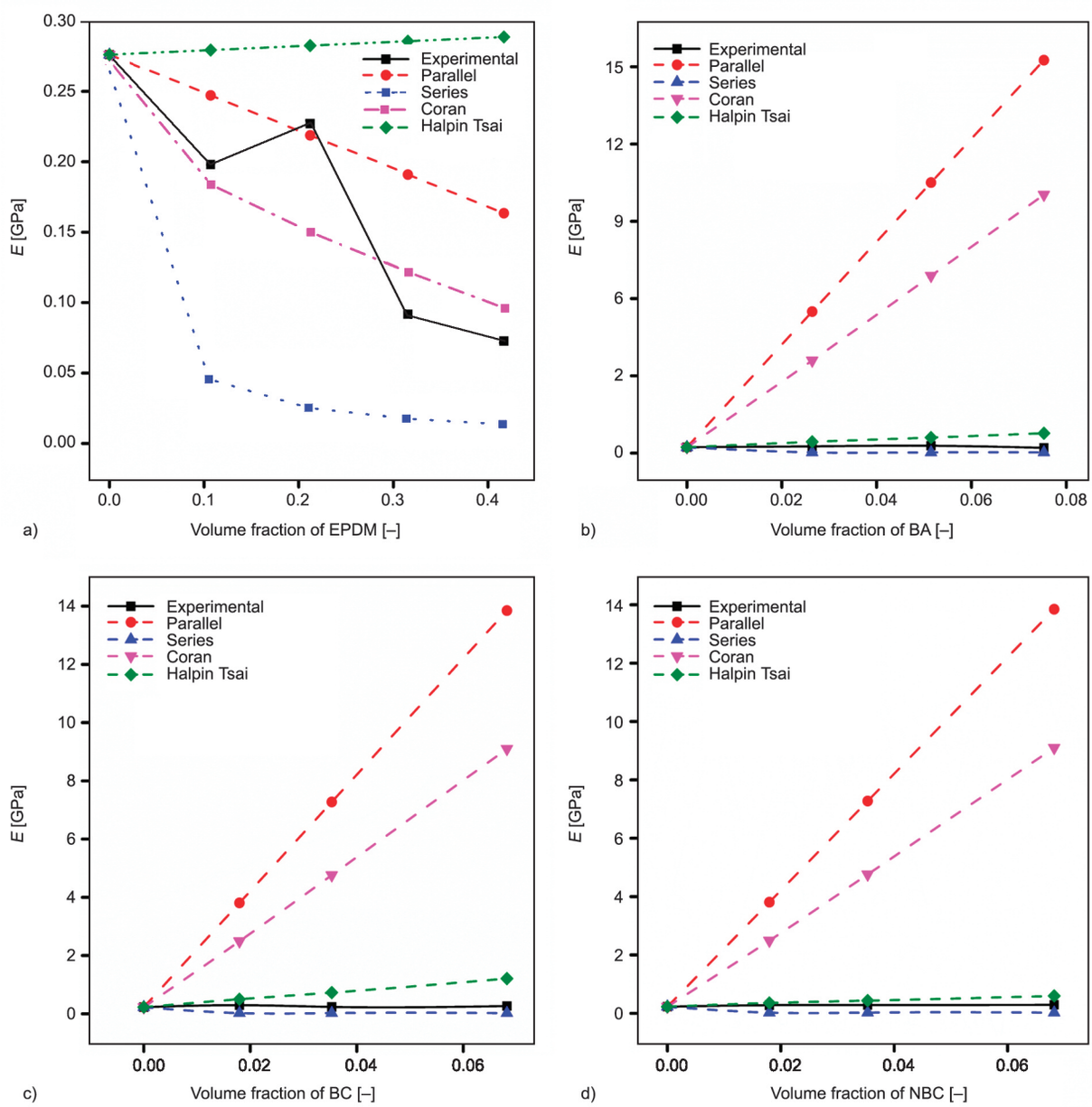

Figure 10. Comparison of Young's modulus values of blends and composites with theoretical models. a) HDPE/EPDM blends with varying volume fraction of EPDM, b) HDPE/EPDM/BA composites with varying volume fraction of BA, c) HDPE/EPDM/BC composites with varying volume fraction of BC, d) DPE/ EPDM/NBC composites with varying volume fraction of NBC.

the enhanced distribution of NBC in the HDPE/ EPDM composites.

3.5. Neutron shielding characteristics

The probability of neutron interaction with the material is given by the macroscopic cross-section of the material. It depends on the atomic density of the material, in which each atom possesses microscopic cross-sections that depend on the interacting neutron energy. Theoretically, the macroscopic cross-section of the samples was calculated using the Lambert-Beer law [16], whose incident and transmitted neutron beam flux [n/cm^2/s] are denoted as I_0 and I, theoretical macroscopic cross-section [cm^2] as Σ and thickness [cm] as t (Equation (7)):

$$I = I_0 \cdot e^{-\Sigma t} \tag{7}$$

where Σ is the sum of the microscopic thermal neutron absorption cross-section σ [cm2/atom] and the atomic number density of the material N [atoms/cm^3] (Equation (8)):

$$\Sigma = \sigma N \quad (8)$$

Neutron permeability (I/I_0) represents the factor of neutron radiations transmitted upon the application of shielding material and it depends on the thickness and energy of incident neutrons. Whereas the average distance travelled by neutrons to encounter an atom in the material is given by the parameter, Mean free path, λ (Equation (9)):

$$\lambda = \frac{1}{\Sigma} \quad (9)$$

Table 4 shows the elemental information of the EP 20 sample *i.e.*, HDPE with 20 wt% EPDM and the corresponding neutron shielding cross-sections at 2 MeV were obtained from the International Atomic Energy Agency: Data File.

The macroscopic cross-section of HDPE is 0.54 cm^{-1}, and the 20 wt% EP 20 blend is 0.48 cm^{-1} corresponding to the 2 MeV energy neutrons. The incorporation of EPDM marginally decreases the macroscopic cross-section. The corresponding hydrogen atomic density of the blends with EPDM loading is represented in Figure 11a. The decrease in the hydrogen atomic density with the addition of EPDM causes this marginal reduction. Because of the small and similar size of the hydrogen atoms and neutrons, collision probability with neutrons is higher if the hydrogen atomic density is higher. For 20 wt% EPDM loading the hydrogen atomic density is $1.409 \cdot 10^{23}$ atom/cm^3. The neutron permeability factor for the 2 mm thickness EP 20 sample is 0.91, and the mean free path is 2.23 cm which resembles a very low ability to attenuate the 2 MeV energy neutrons. Table 4 also illustrates the theoretical neutron attenuation characteristics of BA 15, BC 20, and NBC 20 composite for thermal energy neutrons (0.025 MeV). Composites with 15 wt% BA, 20 wt% BC and NBC show macroscopic cross-section of 5.26, 9.75 and 10 cm^{-1} respectively. A slight increase for the macroscopic cross-section of NBC 20 compared to BC 20 could be due to the better distribution of nanofillers. Boron atoms play a significant role in absorbing thermal energy neutrons due to their high thermal neutron absorption cross-section. The thermal neutron absorption cross-section is proportionally increased with boron atomic density, as shown in Figures 11b, 11c, and 11d. The higher boron atomic density

Table 4. Theoretical neutron attenuation characteristics of EP 20 blend (2 MeV), BA 15 composite (0.025 MeV) and BC 20 composite (0.025 MeV).

Elements	Amount of substance [mol]	Total atoms·10^{23}	Atomic density [atoms/cm^3]·10^{23}	Neutron cross-section [cm^2/atom]·10^{23}	Macroscopic cross-section, σ [cm^{-1}]	Total macroscopic cross-section, Σ [cm^{-1}]	Neutron permeability, I/I_0 at 2 mm	Mean free path, λ [cm]
EP 20 blend for 2 MeV energy neutrons								
C	7.2320	43.55	0.4018	0.171	0.0687	0.48	0.91	2.23
H	25.3644	152.74	1.4092	0.290	0.4087			
O	0	0.00	0.0000	0.158	0.0000			
N	0.0057	0.03	0.0003	0.156	0.0001			
BA 15 composite for 0.025 MeV energy neutrons								
C	7.4746	45.01	0.3840	0.495	0.1901	5.26	0.35	0.19
H	26.0922	157.13	1.3406	3.051	4.0902			
O	0.7278	4.38	0.0374	0.392	0.0146			
N	0.0057	0.03	0.0003	1.219	0.0004			
B	0.2426	1.46	0.0125	77.388	0.9646			
BC 20 composite for 0.025 MeV energy neutrons								
C	7.5940	45.73	0.3830	0.495	0.1897	9.75	0.14	0.1
H	25.3640	152.74	1.2780	3.051	3.9048			
N	0.0057	0.03	0.0003	1.219	0.0004			
B	1.4479	8.72	0.0731	77.388	5.6541			
NBC 20 composite for 0.025 MeV energy neutrons								
C	7.5940	45.73	0.3931	0.495	0.1946	10.00	0.14	0.1
H	25.3640	152.74	1.3128	3.051	4.0055			
N	0.0057	0.03	0.0003	1.219	0.0004			
B	1.4479	8.72	0.0749	77.388	5.7999			

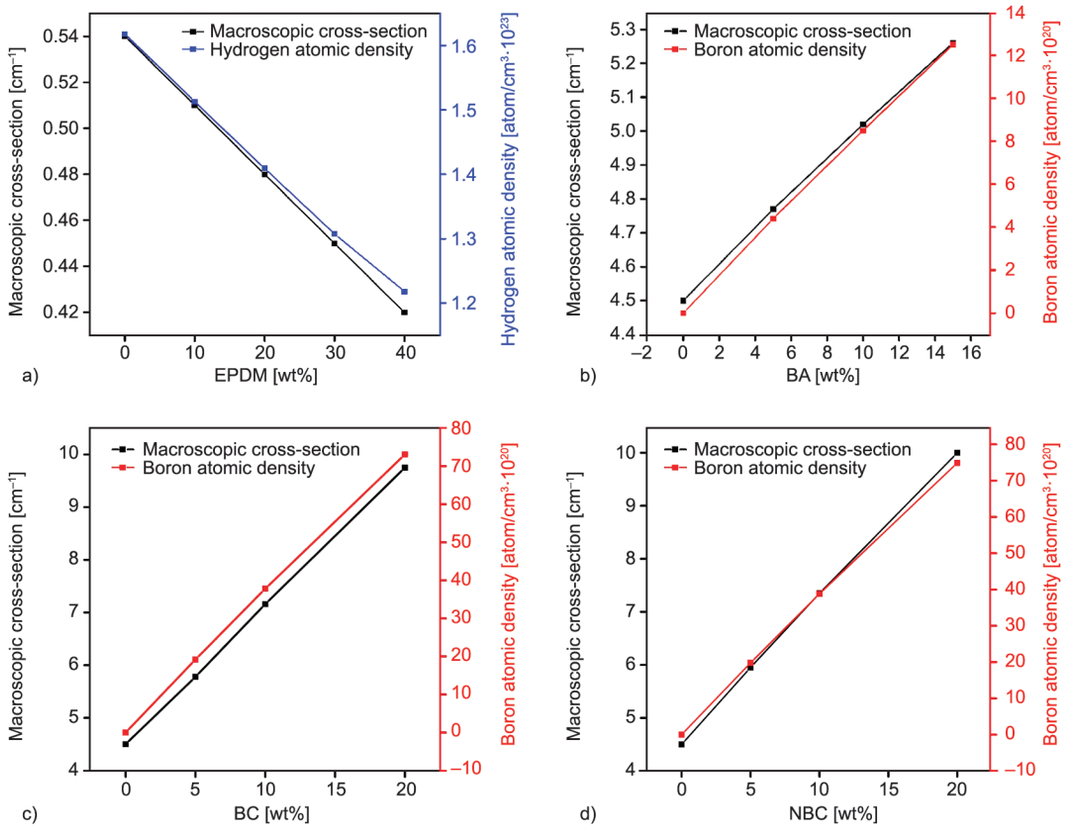

Figure 11. a) Macroscopic cross-section and hydrogen atomic density of the HDPE/EPDM blends with varying EPDM concentration (b), (c) and (d) macroscopic cross-section and boron atomic density of the HDPE/EPDM/ boron compounds with varying BA, BC and NBC respectively.

$7.49 \cdot 10^{21}$ atom/cm^3 for the NBC 20 is the reason for the high neutron absorption cross-section when compared to $1.25 \cdot 10^{21}$ and $7.31 \cdot 10^{21}$ atom/cm^3 for the BA 15 and BC 20, respectively. The neutron permeability for 0.025 MeV neutrons of BA 15 composite at 2 mm thickness is 0.35, and the mean free path is 0.19 cm. This indicates that by applying 2mm thick BA 15 composites 65% of the incident neutrons can attenuate in the neutron shielding applications. In the case of BC 20 and NBC 20, the neutron permeability sharply reduced to 0.14 with a mean free path of 0.1 cm, which shows a reduction of 86% of incident neutrons for 2 mm thickness samples on application.

4. Conclusions

The results of this work demonstrated the development of HDPE/EPDM composites incorporated with BA, BC, and NBC. The influence of the EPDM content in the HDPE matrix indicates that the interparticle distance among dispersed EPDM in HDPE was decreased with EPDM concentration. The addition of EPDM could not modify the crystallization and the melting behaviours of HDPE. Furthermore, the addition of fillers in 20 wt. % EPDM blend has no significant influence on thermal stability and DSC parameters viz. crystallization and the melting behaviours, whatever be the nature and the content of these fillers. Elongation at break [%] and toughness increased with the EPDM incorporation in HDPE, while this causes a corresponding reduction in the tensile strength and modulus. The Young's modulus of the blends followed the trends similar to the Coran model, but 20 wt% EPDM blend resembles the upper bound parallel model indicating better HDPE-EPDM blend morphology. A marginal decrease in the macroscopic cross-section for the elastic collision was observed due to the reduction in hydrogen atomic density with EPDM loading.

BA was noticed to be dispersed in the HDPE phase, and BC shows non-uniform distribution irrespective in the blend. Above 10 wt% BA and BC addition, the tensile strength modulus and toughness of the composites decreased, and the composites represent trends similar to lower bound series models. The nano-sized NBC fillers show the enhanced distribution and tensile characteristics with marginal reduction in toughness. Also, the composites show a better correlation with the Halpin Tsai model, which indicates the effect

of NBC size and shape in the filler distribution in the HDPE/EPDM matrix. The thermal neutron absorption cross-section of the composites enhanced with the boron atomic density. For the same [wt%] of BA, BC, and NBC composites, the macroscopic cross-section was higher for NBC filled composite due to their higher boron content and enhanced distribution.

Acknowledgements

This work was funded by the Department of Atomic Energy, Board of Research in Nuclear Sciences, Government of India under the Grant No. 39/30/2015-BRNS/39010 sanctioned in 2016. Also, the authors are grateful to the European Union and the Normandy Region for the financial support given to the MAGMA project via the 'Fonds Européen de Développement Régional' (FEDER), and to Marie-Rose Garda from Normandie Univ, UNIROUEN Normandie, INSA Rouen, UMR CNRS 6634, Groupe de Physique des Matériaux, 76801 Saint Etienne du Rouvray, France.

References

[1] Mozhayev A. V., Piper R. K., Rathbone B. A., McDonald J. C.: Moderator design studies for a new neutron reference source based on the D-T fusion reaction. Radiation Physics and Chemistry, **123**, 87–96 (2016). https://doi.org/10.1016/j.radphyschem.2016.02.004

[2] Chandra S., Ahmad T., Barth R. F., Kabalka G. W.: Quantitative evaluation of boron neutron capture therapy (BNCT) drugs for boron delivery and retention at subcellular-scale resolution in human glioblastoma cells with imaging secondary ion mass spectrometry (SIMS). Journal of Microscopy, **254**, 146–156 (2014). https://doi.org/10.1111/jmi.12126

[3] McGiff T. J., Danforth R. A., Herschaft E. E.: Maintaining radiation exposures as low as reasonably achievable (ALARA) for dental personnel operating portable handheld X-ray equipment. Health Physics, **103**, S179–S185 (2012). https://doi.org/10.1097/HP.0b013e318259fa29

[4] Orak S., Baysoy D. Y.: Neutron shielding properties of concrete with boron and boron containing mineral. Academic Platform - Journal of Engineering and Science, **1**, 15–19 (2013). https://doi.org/10.5505/apjes.2013.99609

[5] Tanimoto T., Uchida N., Kodama Y., Teshima T., Taniguchi S.: Safety of workers at the Fukushima Daiichi nuclear power plant. The Lancet, **377**, 1489–1490 (2011). https://doi.org/10.1016/S0140-6736(11)60519-9

[6] Rinard P.: Neutron interactions with matter. in 'Passive nondestructive assay of nuclear materials' (eds.: Reilly D., Ensslin N., Smith H Jr., Kreiner S.) Nuclear Regulatory Commission, Washington, 357–377 (1991).

[7] Nambiar S., Yeow J. T. W.: Polymer-composite materials for radiation protection. ACS Applied Materials and Interfaces, **4**, 5717–5726 (2012). https://doi.org/10.1021/am300783d

[8] Sakurai Y., Sasaki A., Kobayashi T.: Development of neutron shielding material using metathesis-polymer matrix. Nuclear Instruments and Methods in Physics Research Section A: Accelerators, Spectrometers, Detectors and Associated Equipment, **522**, 455–461 (2004). https://doi.org/10.1016/j.nima.2003.11.420

[9] Kim J., Uhm Y. R., Lee B., Jung J., Rhee C., Lee M-K., Lee S. H.: Radiation shielding members including nanoparticles as a radiation shielding material and method for preparing the same. U.S. Patent 20100102279A1, USA (2010).

[10] Kim J., Lee B-C., Uhm Y. R., Miller W. H.: Enhancement of thermal neutron attenuation of nano-B4C, -BN dispersed neutron shielding polymer nanocomposites. Journal of Nuclear Materials, **453**, 48–53 (2014). https://doi.org/10.1016/j.jnucmat.2014.06.026

[11] Chiang W-H., Huang S-J., Jang G-W.: Radiation shielding composite material including radiation absorbing material and method for preparing the same. U.S. Patent 20140225039A1, USA (2014).

[12] Harrison C., Weaver S., Bertelsen C., Burgett E., Hertel N., Grulke E.: Polyethylene/boron nitride composites for space radiation shielding. Journal of Applied Polymer Science, **109**, 2529–2538 (2008). https://doi.org/10.1002/app.27949

[13] Shin J. W., Lee J-W., Yu S., Baek B. K., Hong J. P., Seo Y., Kim W. N., Hong S. M., Koo C. M.: Polyethylene/boron-containing composites for radiation shielding. Thermochimica Acta, **585**, 5–9 (2014). https://doi.org/10.1016/j.tca.2014.03.039

[14] Bin Rusayyis M. A., Schiraldi D. A., Maia J.: Property/morphology relationships in SEBS-compatibilized hdpe/poly(phenylene ether) blends. Macromolecules, **51**, 6513–6523 (2018). https://doi.org/10.1021/acs.macromol.8b00894

[15] Özdemir T., Güngör A., Reyhancan A.: Flexible neutron shielding composite material of EPDM rubber with boron trioxide: Mechanical, thermal investigations and neutron shielding tests. Radiation Physics and Chemistry, **131**, 7–12 (2017). https://doi.org/10.1016/j.radphyschem.2016.10.012

[16] Güngör A., Akbay I. K., Özdemir T.: EPDM rubber with hexagonal boron nitride: A thermal neutron shielding composite. Radiation Physics and Chemistry, **165**, 108391 (2019). https://doi.org/10.1016/j.radphyschem.2019.108391

[17] Abdel-Aziz M. M., Gwaily S. E., Makarious A. S., El-Sayed Abdo A.: Ethylene-propylene diene rubber/low density polyethylene/boron carbide composites as neutron shields. Polymer Degradation and Stability, **50**, 235–240 (1995). https://doi.org/10.1016/0141-3910(95)00177-8

[18] Mohamed A. A., Yazid H., Ahmad S.: Experimental optimization in polymer blend composite preparation based on mix level of taguchi robust design. Journal of Nuclear and Related Technologies, **9**, 23–32 (2012).
[19] Zali N. M., Yazid H., Megat Ahmad M. H. A. R.: Neutron shielding behavior of thermoplastic natural rubber/boron carbide composites. IOP Conference Series: Materials Science and Engineering, Selangor, Malaysia, **298**, 012018 (2018).
https://doi.org/10.1088/1757-899X/298/1/012018
[20] Morteza E., Zeynali M. E., Mijtaba A., Harati A. A.: LDPE/EPDM blends as electrical insulators with unique surface, electrical and mechanical properties. Iranian Polymer Journal, **18**, 37–47 (2010).
[21] Stelescu D. M., Airinei A., Homocianu M., Fifere N., Timpu D., Aflori M.: Structural characteristics of some high density polyethylene/EPDM blends. Polymer Testing, **32**, 187–196 (2013).
https://doi.org/10.1016/j.polymertesting.2012.10.010
[22] Özdemir T., Akbay I. K., Uzun H., Reyhancan I. A.: Neutron shielding of EPDM rubber with boric acid: Mechanical, thermal properties and neutron absorption tests. Progress in Nuclear Energy, **89**, 102–109 (2016).
https://doi.org/10.1016/j.pnucene.2016.02.007
[23] Zhang Q., Zhang D., Xu H., Lu W., Ren X., Cai H., Lei H., Huo E., Zhao Y., Qian M., Lin X., Villota E. M., Mateo W.: Biochar filled high-density polyethylene composites with excellent properties: Towards maximizing the utilization of agricultural wastes. Industrial Crops and Products, **146**, 112185 (2020).
https://doi.org/10.1016/j.indcrop.2020.112185
[24] Sharma B. K., Chowdhury S. R., Jha A., Samanta A. K., Mahanwar P., Sarma K. S.: ENGAGE compatibilized HDPE/EPDM blends: Modification of some industrially pertinent properties and morphology upon incorporation of $Mg(OH)_2$ filler and electron beam cross-linked network. Journal of Applied Polymer Science, **134**, 44922 (2017).
https://doi.org/10.1002/app.44922
[25] Naderi G., Lafleur P. G., Dubois C.: The influence of matrix viscosity and composition on the morphology, rheology, and mechanical properties of thermoplastic elastomer nanocomposites based on EPDM/PP. Polymer Composites, **29**, 1301–1309 (2008).
https://doi.org/10.1002/pc.20495
[26] Hajibabazadeh S., Razavi Aghjeh M. K., Palahang M.: Study on the fracture toughness and deformation micromechanisms of PP/EPDM/SiO_2 ternary blend-nanocomposites. Journal of Composite Materials, **54**, 591–605 (2020).
https://doi.org/10.1177/0021998319863475
[27] Zhao P., Gao X., Lu C., Wang X., He Y., Yao D.: Fabricating a partial wetting structure for improving the toughness of intumescent flame-retardant HDPE. Journal of Applied Polymer Science, **137**, 48735 (2020).
https://doi.org/10.1002/app.48735
[28] Kuila T., Srivastava S. K., Bhowmick A. K., Saxena A. K.: Thermoplastic polyolefin based polymer – blend-layered double hydroxide nanocomposites. Composites Science and Technology, **68**, 3234–3239 (2008).
https://doi.org/10.1016/j.compscitech.2008.08.003
[29] Paran S. M. R., Naderi G., Ghoreishy M. H. R., Heydari A.: Enhancement of mechanical, thermal and morphological properties of compatibilized graphene reinforced dynamically vulcanized thermoplastic elastomer vulcanizates based on polyethylene and reclaimed rubber. Composites Science and Technology, **161**, 57–65 (2018).
https://doi.org/10.1016/j.compscitech.2018.04.006
[30] Mishra J. K., Hwang J-K., Ha C-S.: Preparation, mechanical and rheological properties of a thermoplastic polyolefin (TPO)/organoclay nanocomposite with reference to the effect of maleic anhydride modified polypropylene as a compatibilizer. Polymer, **46**, 1995–2002 (2005).
https://doi.org/10.1016/j.polymer.2004.12.044
[31] Fang W., Fei Y., Lu H., Jin J., Zhong M., Fan P., Yang J., Fei Z., Chen F., Kuang T.: Enhanced sound insulation and mechanical properties based on inorganic fillers/thermoplastic elastomer composites. Journal of Thermoplastic Composite Materials, **32**, 936–950 (2019).
https://doi.org/10.1177/0892705718766382
[32] Li X., Wu J., Tang C., He Z., Yuan P., Sun Y., Lau W-M., Zhang K., Mei J., Huang Y.: High temperature resistant polyimide/boron carbide composites for neutron radiation shielding. Composites Part B: Engineering, **159**, 355–361 (2019).
https://doi.org/10.1016/j.compositesb.2018.10.003
[33] Harrison C., Burgett E., Hertel N., Grulke E., El-Genk M. S.: Polyethylene/boron composites for radiation shielding applications. AIP Conference Proceedings, **969**, 484–491(2008).
https://doi.org/10.1063/1.2845006
[34] Uddin Z., Yasin T., Shafiq M., Raza A., Zahur A.: On the physical, chemical, and neutron shielding properties of polyethylene/boron carbide composites. Radiation Physics and Chemistry, **166**, 108450 (2020).
https://doi.org/10.1016/j.radphyschem.2019.108450
[35] Pontón P. I., Yamada K., Guamán M. V., Johnson M. B., White M. A., Marinkovic B. A.: Data supporting micromechanical models for the estimation of Young's modulus and coefficient of thermal expansion of titanate nanotube/$Y_2W_3O_{12}$/HDPE ternary composites. Data in Brief, **25**, 104247 (2019).
https://doi.org/10.1016/j.dib.2019.104247
[36] Pontón P. I., Prisco L. P., Marinkovic B. A.: Effects of low contents of $A_2M_3O_{12}$ submicronic thermomiotic-like fillers on thermal expansion and mechanical properties of HDPE-based composites. Polymer Composites, **39**, E1821–E1833 (2018).
https://doi.org/10.1002/pc.24811
[37] Ostafinska A., Vackova T., Slouf M.: Strong synergistic improvement of mechanical properties in HDPE/COC blends with fibrillar morphology. Polymer Engineering and Science, **58**, 1955–1964 (2018).
https://doi.org/10.1002/pen.24805